https://doi.org/10.5194/egusphere-2023-2429
Preprint. Discussion started: 27 October 2023

Upper Atmosphere Responses to the 2022 Hunga Tonga-Hunga Ha'apai Volcanic Eruption via Acoustic-Gravity Waves and Air-Sea Interaction

Qinzeng Li[1,5], Jiyao Xu[1,2]*, Aditya Riadi Gusman[3], Hanli Liu[4], Wei Yuan[1,5], Weijun Liu[1,5], Yajun Zhu[1,5], and Xiao Liu[6]

1. State Key Laboratory of Space Weather, National Space Science Center, Chinese Academy of Sciences, Beijing, 100190, China
2. School of Astronomy and Space Science, University of Chinese Academy of Science, Beijing, 100049, China
3. GNS Science, Lower Hutt, New Zealand
4. High Altitude Observatory, National Center for Atmospheric Research, Boulder, Colorado, USA
5. Hainan National Field Science Observation and Research Observatory for Space Weather, National Space Science Center, Chinese Academy of Sciences, Beijing, 100190, China
6. School of Mathematics and Information Science, Henan Normal University, Xinxiang, China

Corresponding author: Jiyao Xu (jyxu@swl.ac.cn)

https://doi.org/10.5194/egusphere-2023-2429
Preprint. Discussion started: 27 October 2023

Abstract

Multi-group of strong atmospheric waves (wave packet #1-#5) over China associated with the 2022 Hunga Tonga–Hunga Ha'apai (HTHH) volcano eruptions were observed in the mesopause region using a ground-based airglow network. The phase speed wave packet #1 and wave packet #2 is approximately 312 m/s and 238 m/s respectively, which is consistent with Lamb wave L0 mode and L1 mode from theoretical prediction. The wave fronts of Lamb wave L0 and L1 below the lower thermosphere are vertical, while the wave fronts of L0 mode tilt forward above exhibiting internal wave characteristics, which show good agreement with the theoretical results. Two types of tsunamis were simulated, one type of tsunami is induced by the atmospheric pressure wave (TIAPW) and the other type tsunami is directly induced by the Tonga volcano eruption (TITVE). From backward ray tracing analysis, the TIAPW and TITVE were likely the sources of the acoustic-gravity waves (AGWs) accompanying wave packet #2 and wave packet #4-5, respectively. The scale of tsunamis near the coast is very consistent with the atmospheric AGWs observed by the airglow network. The AGWs triggered by TITVE propagate nearly 3000 km inland with the support of duct and persist for about 4.5 hr and almost covers the Chinese Mainland. The atmospheric pressure wave can directly affect the upper atmosphere, and can also be coupled with the upper atmosphere through the indirect way of generating tsunami and subsequently tsunami generating AGWs, which will provide a new understanding of the coupling between ocean and atmosphere.

https://doi.org/10.5194/egusphere-2023-2429
Preprint. Discussion started: 27 October 2023

1. Introduction

Hunga Tonga–Hunga Ha'apai (HTHH) volcano, which erupted at 04:14:45 UT on January 15, 2022, produced the largest volcanic eruption in terms of energy release of a single event since the Krakatoa volcanic eruption (Symons, 1888) in 1883. This volcanic eruption triggered broad spectrum atmospheric disturbances (Adam, 2022; Duncombe, 2022; Wright et al., 2022), including Lamb waves (Kanamori and Given, 1983, Zhang et al., 2022), acoustic waves, gravity waves (GWs) (Fritts and Alexander, 2003; Liu et al., 2022), and shock waves (Astafyeva et al., 2022). In addition, the travelling ionospheric disturbances (TIDs) caused by this volcanic eruption have also been reported (Themens et al., 2022; Lin et al., 2022).

Lamb waves are external wave propagating along Earth's surface at the speed of sound (Beer, 1974). They are non-dispersive or nearly non-dispersive (Francis, 1973) and can propagate horizontally over long distances. Lamb wave mainly occupies the troposphere, and its perturbation pressure decays exponentially with height (Yeh and Liu, 1974). The Lamb waves excited by the Tonga volcano eruptions went around the Earth several times (Duncombe, 2022; Amores et al., 2022). Liu et al. (2023) reproduced the Lamb wave L0 and L1 modes consistently with theoretical predictions (Francis, 1973) using high-resolution Whole Atmosphere Community Climate Model with thermosphere/ionosphere extension (WACCM-X). Li et al. (2023) identified Lamb wave L1 mode from GNSS TEC analysis.

The 2022 HTHH volcano eruption triggered tsunamis that affected the whole world (Carvajal et al., 2022; Ghent et al., 2022). Tsunamis are typically generated by localized sea surface displacements caused by sources such as earthquakes and volcanoes, similar to the tsunamis directly induced by the 2022 Tonga volcano eruption (TITVE). Another significant mechanism that occurred was the atmospheric pressure wave that excited the tsunamis (Kubota et al., 2022; Gusman et al., 2022). Tsunami can generate upward propagating AGWs through water-air interface and propagate to the height of the thermosphere/ionosphere (Hines, 1972; Peltier and Hines, 1976; Pradipta et al., 2023; Hickey et al., 2009, 2010; Occhippinti et al., 2013; Vadas et al., 2015). Using the red line airglow imager, Makela et al. (2011) detected airglow disturbance in Hawaii that arrived before the tsunami. Also using the redline airglow, Smith et al. (2015) observed sea wave and GW almost simultaneously in Chile. Inchin et al. (2020) used a 3D numerical model to simulate the atmospheric AGWs generated by tsunami. They found that bathymetry variations significantly affected the tsunamis and the AGWs excited by tsunamis, leading to their nonlinear evolution process. More recently, Inchin et al. (2022) simulated the modulation of tsunami induced AGWs on the mesopause airglow radiation, and found that large-scale tsunamis can cause detectable and quantitative disturbances of mesopause airglow through AGWs.

As far as we know, the research on the impact of tsunamis induced atmospheric AGWs on the atmosphere and ionosphere shown above is all caused by conventional tsunami. There are only two studies on the ground-based airglow observations of AGWs caused by this typical type tsunami, and both are limited to red line observations (Makela et al., 2011; Smith et al., 2015). However, the observation of tsunami induced GWs in the mesopause region observed by ground-based airglow imaging has never been reported. Neither has AGWs originate from tsunamis induced by the atmospheric pressure wave (TIAPW) been studied. In this study, we first reported the propagation characteristics of the AGWs generated by the tsunamis triggered by the 2022 HTHH volcano eruptions in the mesopause region using the

https://doi.org/10.5194/egusphere-2023-2429
Preprint. Discussion started: 27 October 2023

ground-based airglow observation network. We then focus on the coupling process of atmospheric pressure waves triggering tsunamis, and then tsunamis generating atmospheric AGWs (air-water-air-coupling process) in the far-field area of the 2022 HTHH volcano eruption.

2. Data and Methods

2.1 Double layer airglow network

A multi-layer airglow observation network (Xu et al., 2021) was built to study atmospheric disturbances excited by severe weather events, such as thunderstorms (Xu et al., 2015), typhoons (Li et al., 2022) and volcanic activities. The multi-layer airglow observation network mainly includes the OH airglow network, which has been used to observe the airglow layer at the height of 87 km; the OI airglow network has been used to observe the airglow layer at the height of 250 km. In addition, there were 557 nm airglow and Na airglow imagers installed at some stations, such as Xinglong Station. The airglow network can provide observation with high temporal and spatial resolution. The temporal resolution is 1 min and the spatial resolution is 1 km. The airglow image was calibrated with the help of standard star map and projected into geospatial space. The background radiation is removed by differential method, to highlight atmospheric fluctuations.

2.2 Tsunami simulation model

Tonga submarine volcano erupted on 15 January 2022, and generated tsunamis that were detected around the globe, affected particularly the Pacific region. In this study, two types of tsunamis were simulated, conventional tsunami simulations and atmospheric pressure wave-induced tsunami simulations. For the tsunami simulations from a localized source, a

B-spline function (Koketsu and Higashi, 1992) is used to represent the circular water uplift source at the volcano. For the second type of tsunami source, the atmospheric pressure wave model is based on the Equation (1) in Gusman et al. (2022). The moving change pressure terms as an input to tsunami simulation momentum equation. For detailed tsunami simulation algorithms, please refer to Gusman et al. (2022).

2.3 Ray tracing method

The following ray tracing equations (Lighthill, 1978) describes the propagation path of AGWs.

$$\frac{dx_i}{dt} = \frac{\partial \omega}{\partial k_i} = c_{g_i} \qquad (1)$$

$$\frac{dk_i}{dt} = -\frac{\partial \omega}{\partial x_i} \qquad (2)$$

There is no real-time temperature data available in this study. Temperature data used to study the propagation characteristics of AGWs is from the Sounding of the Atmosphere using Broad band Emission Radiometry (SABER) instrument on the Thermosphere Ionosphere Mesosphere Energetics and Dynamics (TIMED) satellite. There are three TIMED satellite tracks with descending track at about 12:07 UT and ascending track at about 21:18 UT and with ascending track at about 22:54 UT inland China as shown in Fig.7a. Using the dispersion relation of acoustic gravity wave (Yeh and Liu, 1974), we can assess the vertical propagation state of AGWs. The dispersion relation is as follows

$$m^2 = \frac{\omega^2}{c_s^2}(1-\frac{\omega_a^2}{\omega^2}) - k^2(1-\frac{\omega_b^2}{\omega^2}) \qquad (3)$$

where m is the vertical wave number, k is the horizontal wave number, c_s the local speed of sound, $\omega = k(c-u)$ is intrinsic frequency, c is the horizontal phase speed, u is the background wind speed in the direction of wave propagation from Horizontal Wind Model 14 (HWM-14)

https://doi.org/10.5194/egusphere-2023-2429
Preprint. Discussion started: 27 October 2023

(Drob et al., 2015). $\omega_a^2 = \frac{g}{T}\frac{dT}{dz} + \frac{\gamma g}{4H}$ is acoustic cutoff frequency, $\omega_b^2 = \frac{g}{T}\frac{dT}{dz} + \frac{(\gamma-1)g}{\gamma H}$ is buoyancy frequency, g is the gravitational acceleration, and T is temperature from the SABER/ TIMED satellite observation. When $\omega>\omega_a$ or $\omega<\omega_b$, $m^2> 0$, AGW can propagate freely, while when $\omega_b<\omega<\omega_a$, $m^2< 0$, the wave is evanescent.

3. Results and Discussion

3.1 Upper Atmospheric Airglow Responses to HTHH Volcanic Eruption via Lamb Waves

Five groups of atmospheric waves (wave packet #1-5) were observed in the mesopause region by the ground-based airglow network. Figure 1 shows the wave packet #1 observed at each station of the OH airglow network (top panels). Wave packet #1 entered the view of the OH airglow network approximately 8 hr after the HTHH volcanic eruption. Three hours after wave packet #1 entered the field of view, wave packet #2 was observed by the OH airglow network. The leading front of wave packet #2 has an uninterrupted continuous front, which almost covers the whole Chinese Mainland (middle panels). Interestingly, we observed AGWs accompanying wave packet #2 (hereafter wave packet #3) over the northwest region of the Yellow Sea (Middle image of middle panels). Wave packet #2 always keeps a stable state in the process of propagation, and maintains a regular front when propagating over Lhasa Station (29.7ºN, 91.0 ºE). Wave packet #4 exhibits strong instability characteristics during propagation. Compared to the continuous leading front of wave packet #2, the fronts of wave packet #4 and #5 are separated (bottom panels). We also found that wave packet #5 (Left image of bottom panels) propagate more than 3000 km inland (propagating to the area west of longitude 90°E).

https://doi.org/10.5194/egusphere-2023-2429
Preprint. Discussion started: 27 October 2023

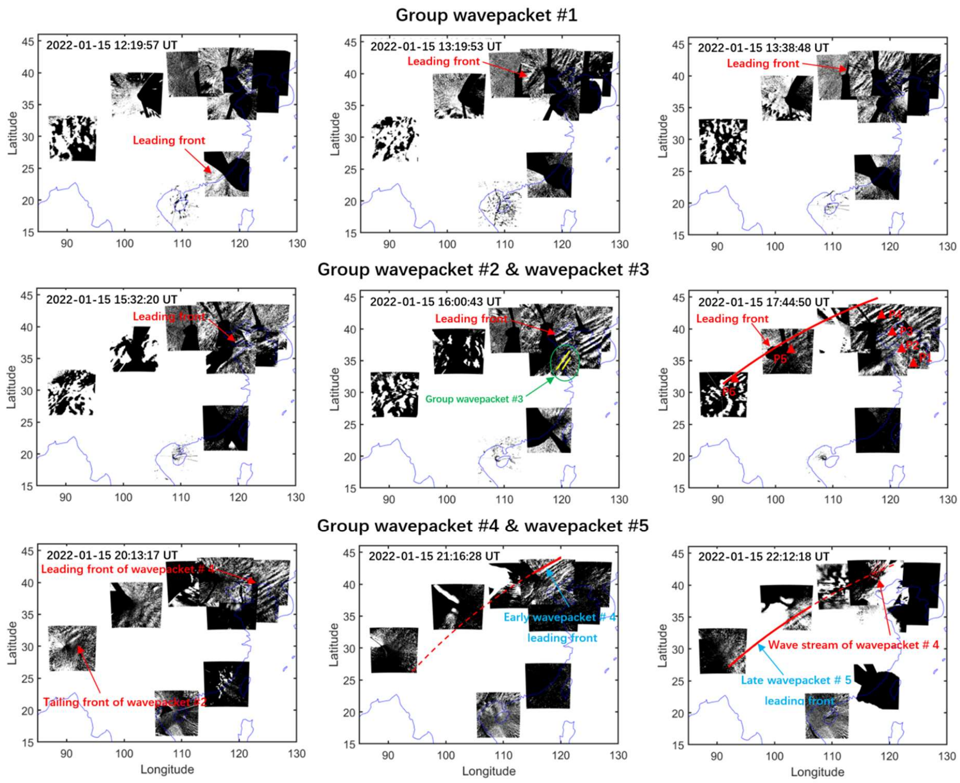

Figure 1 Five strong group atmospheric waves associated with the Tonga volcano eruptions were observed in the mesopause region by the ground-based airglow network.

Figure 2 shows the relationship between horizontal phases speed and relative amplitude and longitude. The phase speed of wave packet #1 is approximately 312 m/s. Wave packet #2 displays a slightly slower phase speed, with average phase speed of 238 m/s. The horizontal phase velocity of group wave packet # 4-5 is less than that of the first GW, which is approximately 207 m/s. For wave amplitude, the relative amplitude of wave packet #2 is greater than that of wave packets #1 and # 4-5, with a maximum amplitude of nearly 30%, and wave packet #4-5 has the smallest relative amplitude.

https://doi.org/10.5194/egusphere-2023-2429
Preprint. Discussion started: 27 October 2023

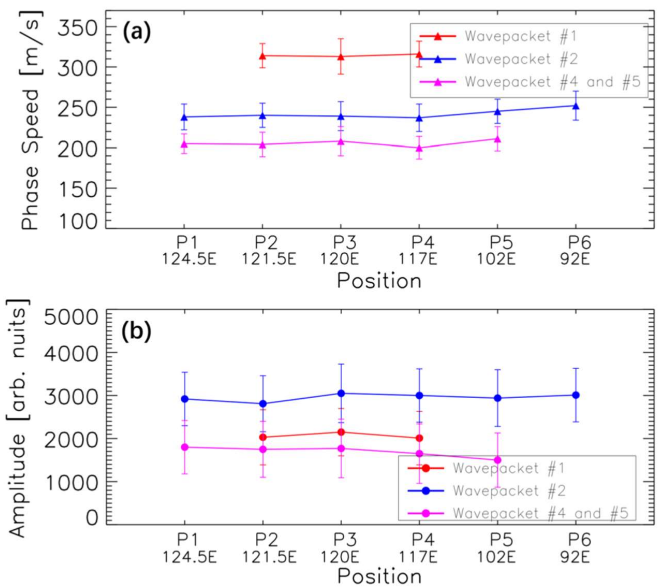

Figure 2 Variation of (a) phase speed and (b) relative amplitude of GWs with longitude.

The HTHH volcano eruption produced Lamb waves that propagate around the globe[4], causing sudden changes in surface pressure. Figure 3 shows vertical distribution characteristics of atmospheric waves caused by Tonga volcano eruption from the surface to the thermosphere atmosphere. Figure 3d shows the surface air pressure data of Xinglong station (40.4ºN, 117.6 ºE). At 13:15 UT on January 15, 2022, the air pressure dropped sharply from 920 Pa to 917.7 Pa, indicating that Lamb wave arrived at the surface of Xinglong station at 13:15 UT. A small disturbance of air pressure occurs at 16:33 UT. The time when wave packet #1 (Fig. 3b) and wave packet #2 (Fig. 3c) reach the zenith direction of Xinglong Station from OH airglow observation is 13:13:34 UT and 16:32:16 UT, which matches the time for surface pressure disturbances quite well. The phase speed of the wave packet #1 (~312 m/s) is very close to the speed of surface Lamb wave (L0 mode). The wave packet # 2 with a slower phase speed (~238 m/s) is consistent with the Lamb wave L1 mode in theoretical predictions

https://doi.org/10.5194/egusphere-2023-2429
Preprint. Discussion started: 27 October 2023

(Francis, 1973) and simulations from WACCM-X model (Liu et al., 2023). However, at almost the same time, the wave front observed in the thermosphere with a slightly faster phase speed of 342 m/s is nearly 550 km a head of the wave front in the mesopause region in the horizontal propagation direction and ahead of time approximately 30 min (Fig. 3a). This is in good agreement with theoretical and modeling results (Fig. 4 of Lindzen and Blake, 1972; Fig. 2 of Liu et al. 2023), which show that the wave fronts of Lamb wave L0 below the lower thermosphere are vertical and tilt forward above. As for Lamb wave L1 mode, the ground and mesopause region provide waveguide surfaces, resulting in maximum wave energy between the two layer, while the phase does not change with height (Francis, 1973).

As mentioned above, the amplitude of Lamb wave L1 mode in the mesopause region is greater than that of L0 mode, which may be due to the fact that L1 mode is an internal wave below the mesopause (Liu et al. 2023). For an isothermal atmosphere, the Lamb wave L0 mode amplitude grows with altitude z as $e^{\kappa z/H}$,where H is the scale height, $\kappa = (\gamma - 1)/\gamma$, and γ is the ratio of specific heats (~1.4). However, the amplitude of internal GWs varies as $e^{z/2H}$. The amplitude of internal waves increases with height at a rate greater than that of surface modes.

https://doi.org/10.5194/egusphere-2023-2429
Preprint. Discussion started: 27 October 2023

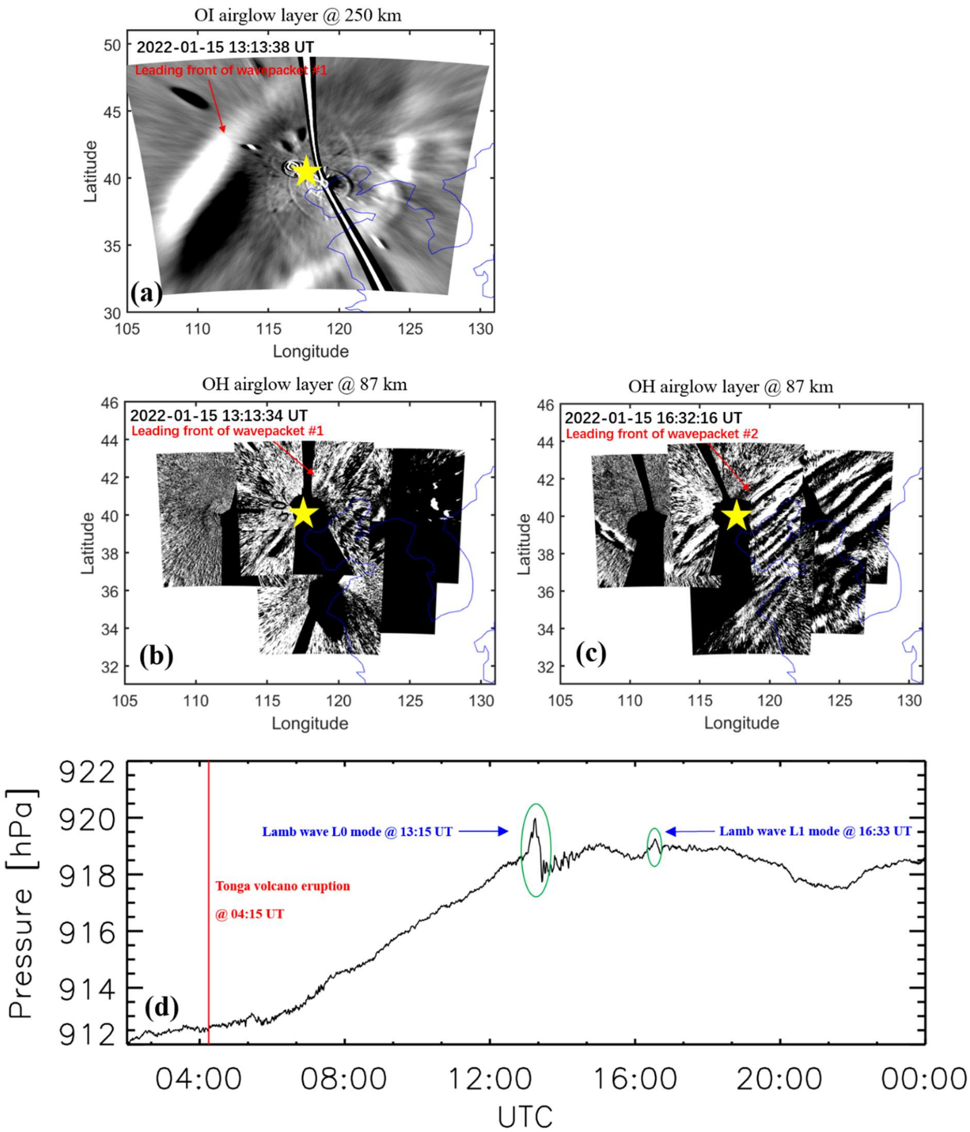

Figure 3 (a) OI 630 nm airglow observation at 13:13:18 UT. OH airglow network observations when (b) wave packet #1 and (c) wave packet #2 pass through the zenith direction of Xinglong Station at 13:13:34 UT and at 16:32:16 UT, respectively. (d)The surface pressure profile obtained from Xinglong observation station. The sudden change of air pressure at 13:15 UT indicates the arrival time of Lamb wave L0. A small disturbance of air pressure occurs at 16:33 UT indicates the arrival time of Lamb wave L1. The yellow stars represent the position of the Xinglong station.

https://doi.org/10.5194/egusphere-2023-2429
Preprint. Discussion started: 27 October 2023

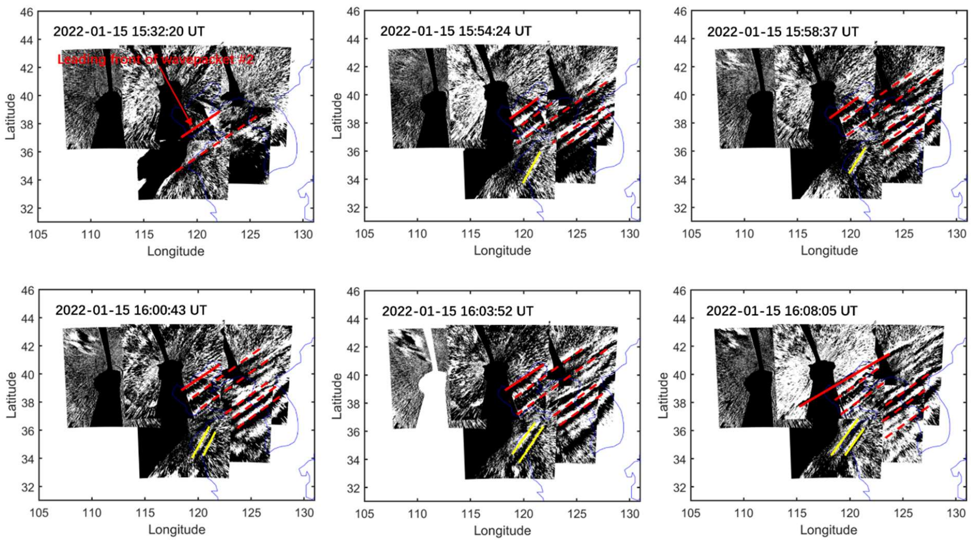

Figure 4 The red solid lines indicate leading wave front of the wave packet #2. The yellow solid line marks other wave fronts, which are clearly not parallel to the wave fronts of wave packet #2.

Figure 4 shows the time sequence of propagation image of wave packet #3. We found that with the propagation of wave packet #2, there is an AGW with a certain angle between its phase plane and the phase plane of wave packet #2. This implies that the source of the wave packet #3 is different from that of wave packet #2. The horizontal wavelength of the wave packet #3 near the coast is 84 km ± 5 km. We find the horizontal wavelengths of the atmospheric AGW observed by airglow network are very consistent with the simulated tsunamis near the coast.

3.2 Simulation of Tsunami induced by HTHH Volcano Eruption

The 2022 HTHH volcano eruption triggered global atmospheric pressure waves. The simulated atmospheric pressure waves propagateat an approximate constant speed of 317 m/s, and the amplitude decreases with the distance from the volcano(Gusman et al., 2022). Figure 5 shows snapshots of the TIAPW and TITVE simulation results. The leading TIAPW excited by

https://doi.org/10.5194/egusphere-2023-2429
Preprint. Discussion started: 27 October 2023

the pressure disturbances travels at the same speed as the atmospheric pressure wave. The propagation speed of TITVE from the shallow water (long) wave approximation is $v=\sqrt{gH_0}$ (Salmon, 2014), where g is the gravitational acceleration and H_0 is the ocean depth. For sea water with a general depth of 4 km, the speed of shallow water wave is about 200 m/s. Therefore, the TIAPW is significantly faster than the TITVE. We found that the TIAPW arrived along the coast of Chinese Mainland about 4-5 hours earlier than the TITVE. However, in the relatively shallow Yellow Sea, the leading TIAPW is very small and only the later waves of the TIAPW are relatively large.

https://doi.org/10.5194/egusphere-2023-2429
Preprint. Discussion started: 27 October 2023

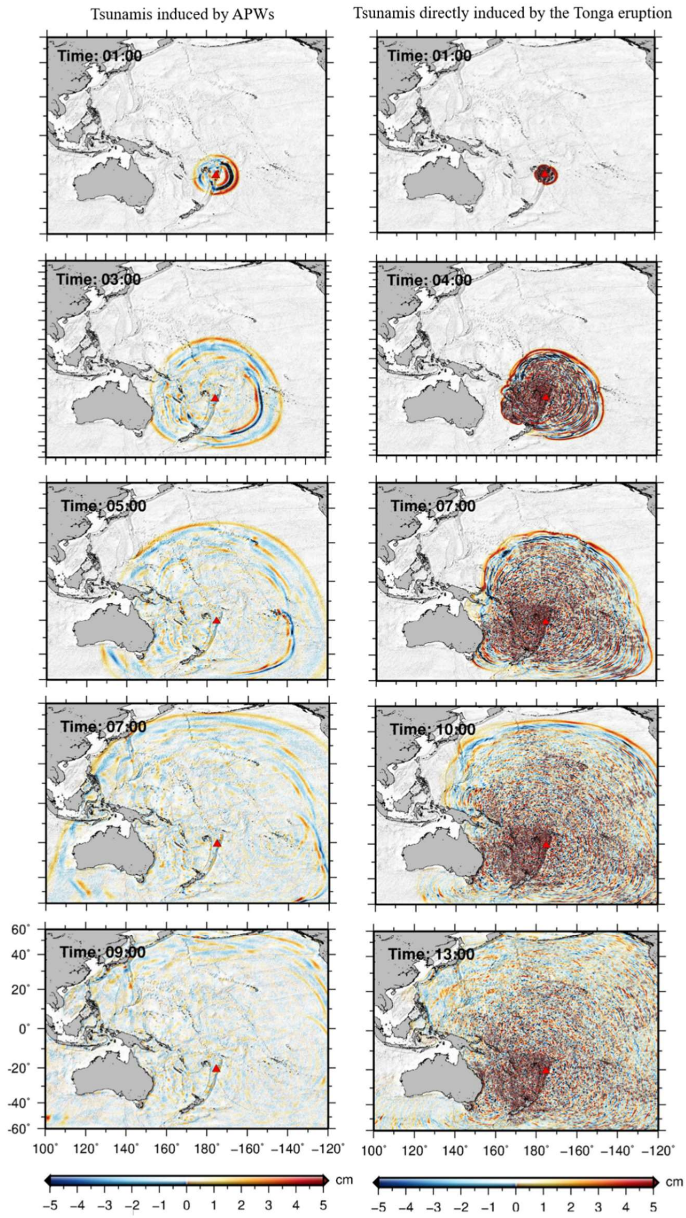

Figure 5 Snapshots of simulated tsunamis induced by the atmospheric pressure wave (left panels) and tsunamis directly induced by the Tonga volcano eruption (right panels).

3.3 Upper atmosphere responses to HTHH volcanic eruption via Air-Sea Interaction

Figure 6 shows the simulation results of TIAPW and TITVE near the coast of Chinese

Mainland11 hr (15:15 UT) and 15 hr (19:15 UT) after the volcanic eruption, respectively. Air pressure waves are not very efficient at directly exciting tsunamis in shallow water due to the weaker air-sea coupling (Gusman et al., 2022; Yamada et al., 2022). The Yellow sea is quite shallow, so the amplitude of the leading of TIAPW is very small there. The leading wave is followed by subsequent waves with larger amplitudes, which propagate in the same direction as the leading wave but at the conventional tsunami speed (Gusman et al., 2022). We found that the TIAPW and TITVE on the continental shelf have shorter wavelengths compared with those in the deep ocean. When the tsunamis approached the coast of China, three groups of AGWs (wave packet #3 and wave packet #4-5) were observed by the airglow network. The time when the AGW entered the view of the airglow network was very close to the time when the Tonga tsunamis reached the coast of Chinese Mainland. The wave packet #3 entered the airglow network at 15:30 UT and the wave packet #4-5 entered the airglow network at 19:40 UT. This strongly suggests that the wave packets detected by the airglow network are correlated to the tsunamis near the coast. We found that as the tsunamis approached the coast of China, they diffracted between Taiwan and Philippines and became discontinuous. And the wave packet #4 and #5 we observed was also discontinuous, which further confirms the correlation between wave packet # 4-5 and discontinuous tsunamis. We estimate that the average wavelength of TIAPW near the coast of the Yellow Sea is approximately 82 km ± 4 km, while the average wavelengths of TITVE near the coast of the Yellow Sea and South Sea are 95 ± 5 km and 86 ± 5 km, respectively.

https://doi.org/10.5194/egusphere-2023-2429
Preprint. Discussion started: 27 October 2023

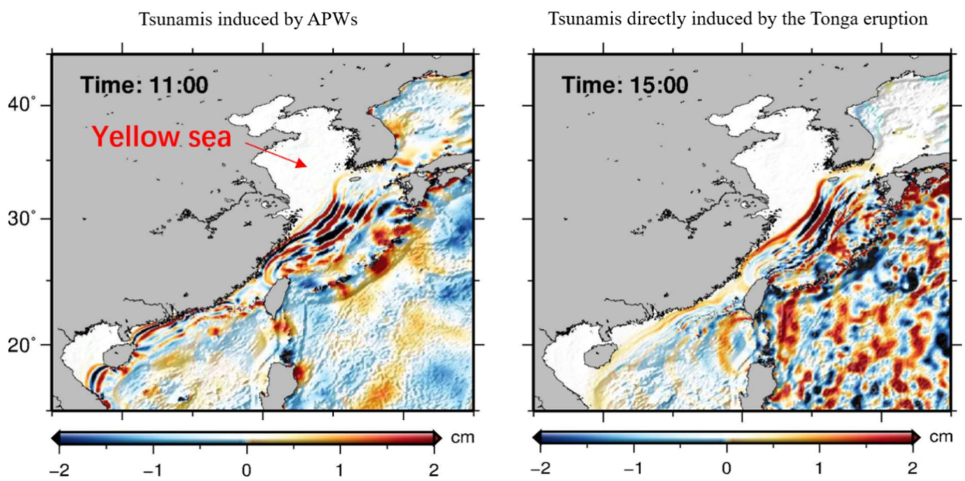

Figure 6 Simulated tsunamis induced by the atmospheric pressure wave (left panels) and tsunamis directly induced by the Tonga volcano eruption (right panels) near the coast of Chinese Mainland. The marked time represents the time after the volcanic eruption.

Figure 7b shows the square of vertical wave number m^2 profile (black) derived from the average temperature from the limb viewing of the Sounding of the Atmosphere using SABER/ TIMED measurement locations marked by the red circles and triangles in Fig.7a. We take the average temperature of ascending track #1and descending track #1 serves as the background temperature for the wave packet #3 and ascending track #1 as the background temperature of the wave packet #3 when they propagate in the coastal vicinity. We take ascending track #2 as the background temperature of wave packet #3 when they propagate inland China. The wind field is from ERA-5 (Hersbach et al., 2020) and HWM-14. The peak height of OH airglow layer is 87 km. We found that the propagation of wave packet #3 (dash-dotted line) is in a state of free propagation in the coastal vicinity.

Figure 8 shows the results of ray tracing for the wave packet #3. We find that the source location of AGWs over the coast of Chinese Mainland falls in the near coast where the tsunami occurred. Therefore, we suggest that the waves with larger amplitudes following the leading of TIAPW interact with the atmosphere after arriving at the coast of Chinese Mainland to generate the upward propagating AGW packet.

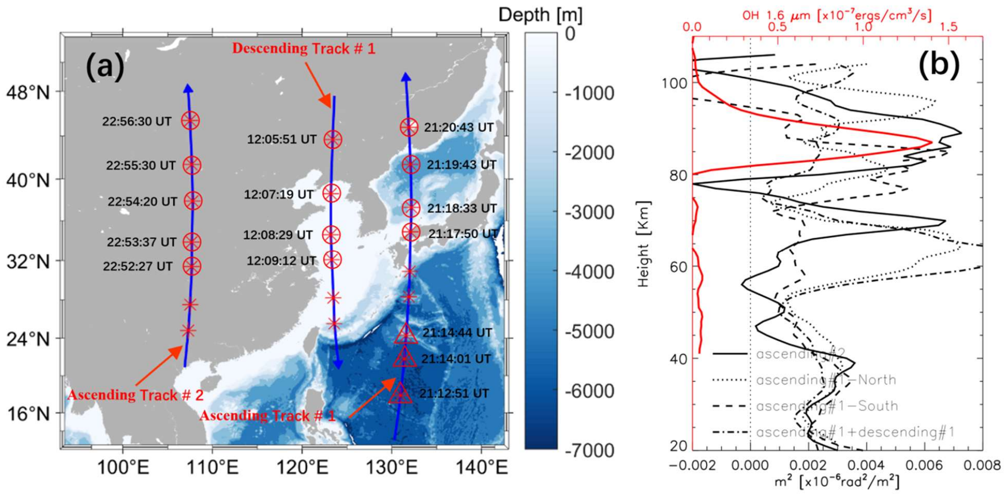

Figure 7 (a) Ascending and descending SABER/TIMED satellite tracks over Chinese Mainland. Background representative ocean depth map. (b) Square of vertical wave number m^2 profiles: black solid line profile derived from the ascending track #2 (marked by the red circle), dotted line profile derived from the ascending track #1-North (marked by the red circle), dashed line profile derived from the ascending track #1-South (marked by the red triangle), and dash-dotted line profile derived from the average the ascending track #1 and descending track #1 (marked by the red circle) from the SABER/TIMED measurement locations in (a). The red line represents the OH 1.6 μm emission intensity obtained by the SABER/TIMED.

https://doi.org/10.5194/egusphere-2023-2429
Preprint. Discussion started: 27 October 2023

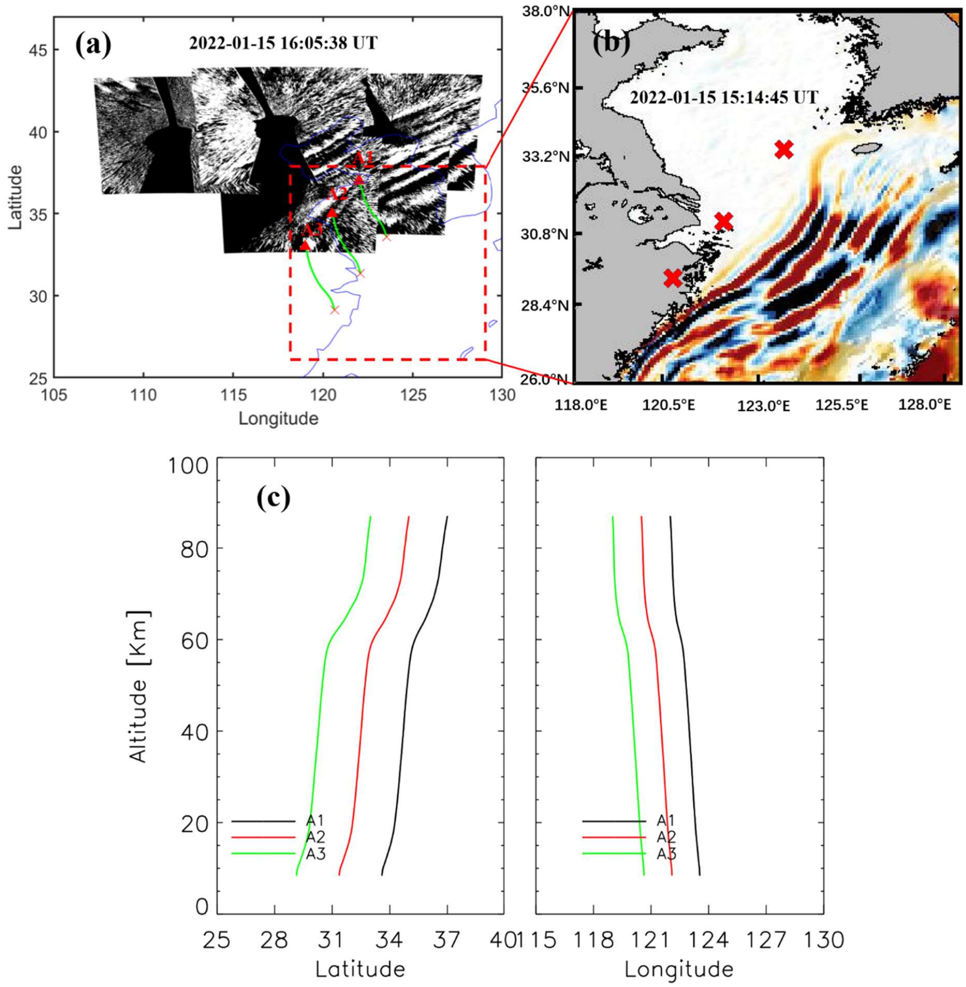

Figure 8 (a) Backward ray tracing results of the wave packet #3 observed by the OH airglow network. The red triangles and red crosses represent the trace start and termination points, respectively. (b) Simulated tsunamis induced by the atmospheric pressure wave (TIAPW) corresponding to the dotted rectangular area in (a). (c) Ray paths of the wave starting from the seven sampling points in (a).

According to the theory of AGW dispersion, the AGW propagating obliquely has the following approximate relationship: $\sin(\varphi) \sim T_B / T$, φ is the oblique propagation angle, T_B is the buoyancy period, T is the intrinsic period. Azeem et al. (2007) found that the disturbances in the ionosphere excited by the 2011 Tohoku tsunamis when they reached the west coast of the United States. They concluded that the fluctuations observed in TEC satisfy

https://doi.org/10.5194/egusphere-2023-2429
Preprint. Discussion started: 27 October 2023

AGW dispersion relation, and the period and horizontal wavelength of the TEC disturbances increased with distance from the West Coast of the U.S.

From the airglow network observations, we found that the wave packet #4-5 excited by the tsunamis, continues to propagate over the main land more than 3000 km from the coast. If the AGWs observed by the airglow network satisfy the dispersion relation, we will obtain the propagation characteristics similar to that observed by Azeem et al. (2007) in the ionosphere from TEC observations. T_B is about 5min from the SABER/TIMED observation. The period of wave packet #3 is between 5.5 min and 8.5 min. The minimum propagation angle φ equals 35°, and the corresponding maximum propagation distance L is 125 km from $L \sim H_{oh}/\tan(\varphi)$ estimation, where H_{oh}=87 km is the height of OH airglow layer. However, our observation does not satisfy the free oblique propagation dispersion theory of AGWs. In addition, we did not find that the GW horizontal wavelength increased with the distance from the shore, as predicted by the theory of AGW oblique propagation. Therefore, the AGWs excited by the tsunami we observed in the mesopause region may be modulated by duct.

We did find a duct structure between 80 and 93 km (black solid line in Fig. 7b), while the wave packet #3 were in a state of free propagation when they propagate around the coastal vicinity of Chinese Mainland (dotted line and dashed line). The duct almost includes the whole OH airglow layer. Therefore, we believe that AGWs generated by TITVE may enter the duct in the process of propagation over Chinese Mainland. The duct structure over Chinese Mainland can explain that the GWs generated by the tsunamis can propagate thousands of kilometers inland.

Figure 9 shows the results of ray tracing for wave packet #4-5. The horizontal

https://doi.org/10.5194/egusphere-2023-2429
Preprint. Discussion started: 27 October 2023

wavelength of wave packet #4 and #5 observed near the coast by the OH airglow network approximately 89 km ± 6 km and 80 km ± 4 km. We find that the source location of AGWs over the coast of Chinese Mainland falls in the near tsunami area, while the location of AGW ray termination over the inland (position B6 and B7 in Fig. 9d) is around 80 km, which indicates that the wave meets the evanescent layer (Wrasse et al., 2006). This is consistent with the duct structure obtained through dispersion relation. Therefore, we suggest that TITVE interact with the atmosphere after arriving at the coast of Chinese Mainland to generate the upward propagating AGW packet. After reaching the mesopause region, this wave packet enters the wave duct structure in the horizontal propagation process, and this wave duct supports wave packet #3 to propagate more than 3000 km inland China.

https://doi.org/10.5194/egusphere-2023-2429
Preprint. Discussion started: 27 October 2023

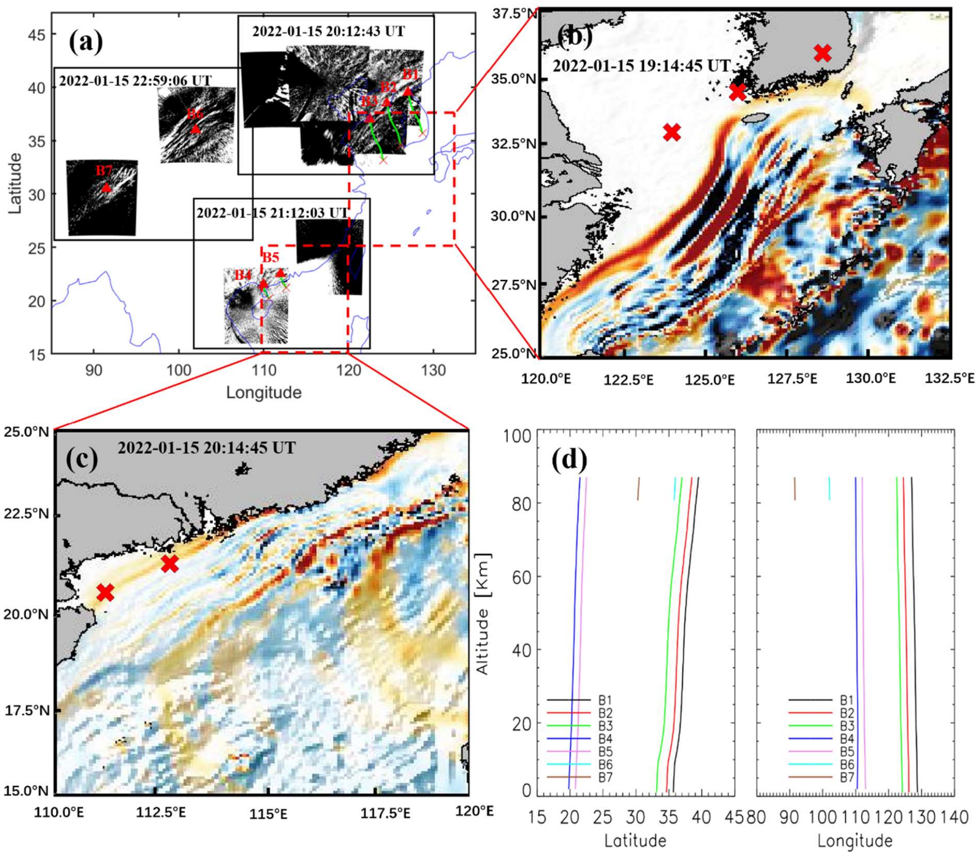

Figure 9 (a) Backward ray tracing results of the fourth and five group GWs observed by the OH airglow network. The red triangles and red crosses represent the trace start and termination points, respectively. (b) and (c) Simulated tsunami directly induced by the Tonga volcano eruption (SWITVE) corresponding to the dotted rectangular area in (a). (c) Ray paths of the wave starting from the seven sampling points in (a).

4. Conclusions

Strong atmospheric disturbances, including Lamb waves, acoustic waves, and gravity waves, were triggered by the 2022 HTHH volcano eruption. The HTHH submarine volcanic eruption also triggered an unusual tsunami, which can generate atmospheric gravity waves (Fig. 10). We observed five strong group atmospheric waves associated with the HTHH volcano eruption from the ground-based airglow network observations.

The phase speed of the wave packet #1 is approximately 312 m/s, which is observed

https://doi.org/10.5194/egusphere-2023-2429
Preprint. Discussion started: 27 October 2023

almost simultaneously with the surface Lamb wave L0 mode. Wave packet #2, with average phase speed of 238 m/s, has been confirmed as Lamb wave L1 mode from theoretical prediction. Wave packet # 3 and wave packet #4-5 are generated by TIAPW and TITVE from backward ray tracing analysis. The horizontal phase speed of the wave packet #4-5 is less than that of the wave packet #1 and wave packet #2, which is approximately 207 m/s. The horizontal wavelengths of the atmospheric AGWs observed by the airglow network are very consistent with those of the tsunami near the coast. This is the first time that we observed the AGWs triggered by the oceanic waves in the mesopause region using optical detection equipment. It is also the first time to report atmospheric gravity waves excited by TIAPW.

The AGWs generated by TITVE propagate nearly 3000 km inland and almost covers the entire Chinese Mainland. When the wave excited by TITVE propagate far away from the coast, the characteristics of AGWs are not consistent with the dispersion of free propagation AGWs. We find these wave packets are controlled by the duct, which can support the propagation of these GWs for thousands of kilometers after the tsunami were stopped at the coast. Therefore, ocean waves can have a significant impact on the upper atmosphere over inland areas far from the ocean through AGWs.

The surface atmospheric pressure wave generated by the 2022 HTHH volcano eruption can directly affect the upper atmosphere. The atmospheric pressure wave from the eruption generated a fast tsunami never before observed by tsunami observation networks. When the tsunamis reach the coast, their speeds decrease but their amplitudes increase, and the atmospheric gravity wave generated by them will also affect the upper atmosphere. Therefore, it exhibits special dynamic coupling process between air and sea via acoustic gravity waves

https://doi.org/10.5194/egusphere-2023-2429
Preprint. Discussion started: 27 October 2023

(Fig. 10). This indirect impact on the upper atmosphere provides a new perspective for us to study the coupling between the ocean and the atmosphere.

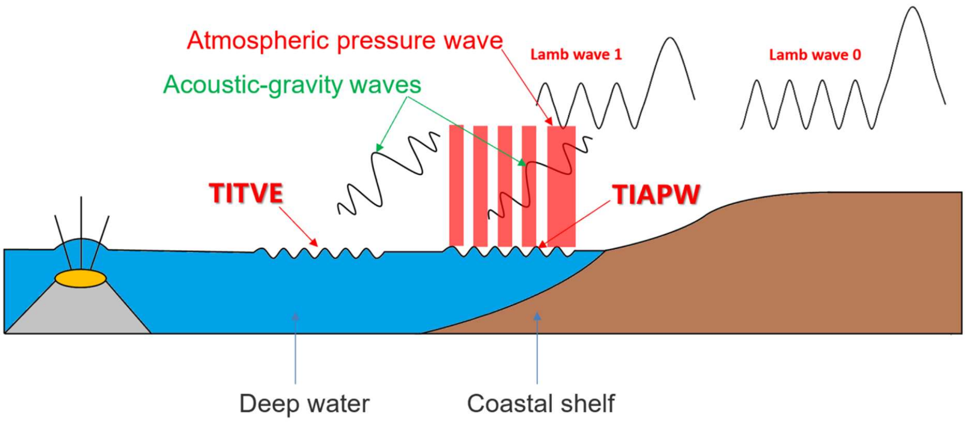

Figure 10 The Tonga volcano eruptions triggered two types of tsunamis, one type of tsunami is induced by the atmospheric pressure wave (TIAPW) and the other type tsunami is directly induced by the Tonga volcano eruption (TITVE). The acoustic gravity waves (AGWs) caused by tsunamis can propagate to the mesopause region.

Data availability

The Double Layer Airglow Network data is available at https://data2.meridianproject.ac.cn/data. TIMED/SABER data is accessed from http://saber.gats-inc.com/data.php. The ERA5 reanalysis data are able to be downloaded from the Copernicus Climate Change Service Climate Data Store through https://www.ecmwf.int/en/forecasts/datasets/reanalysis-datasets/era5.

Author contributions

J.X and Q.L. conceived the idea of the manuscript. Q.L. carried out the data analysis, interpretation and manuscript preparation. A.R.G. developed and performed the numerical simulations. W.L and Y.Z compiled, processed and analysed satellite data. H.L.L., X.L and

https://doi.org/10.5194/egusphere-2023-2429
Preprint. Discussion started: 27 October 2023

W.Y. contributed to the data interpretation and manuscript preparation. All authors discussed the results and commented on the manuscript.

Competing interests

The authors declare no competing interests.

Acknowledgements

This work was supported by the National Science Foundation of China (42374205, 41831073 and 41974179). The project is also supported by the Specialized Research Fund for State Key Laboratories. We acknowledge the use of data from the Chinese Meridian Project.

References

Adam, D.: Tonga volcano eruption created puzzling ripples in Earth’s atmosphere, Nature, 601, 497, 2022.

Amores, A., Monserrat, S., Marcos, M., Argüeso, D., Villalonga, J., Jordà, G., and Gomis, D.: Numerical simulation of atmospheric Lamb waves generated by the 2022 Hunga-Tonga volcanic eruption, Geophysical Research Letters, 49, 2022.

Astafyeva, E., Maletckii, B., Mikesell, T. D., Munaibari, E., Ravanelli, M., Coisson, P., et al. The 15 January 2022 Hunga Tonga eruption history as inferred from ionospheric observations, Geophysical Research Letters, 49, 2022.

Azeem, I., Vadas, S. L., Crowley, G., and Makela, J. J.: Traveling ionospheric disturbances over the United States induced by gravity waves from the 2011Tohoku tsunami and comparison with gravity wave dissipative theory, J. Geophys. Res. Space Physics, 122,

https://doi.org/10.5194/egusphere-2023-2429
Preprint. Discussion started: 27 October 2023

3430–3447, 2017.

Beer, T. Atmospheric Waves, 300 pp., John Wiley, New York, 1974.

Carvajal, M., Sepúlveda, I., Gubler, A., and Garreaud, R. Worldwide signature of the 2022 Tonga volcanic tsunami, Geophysical Research Letters, 49(6), 2022.

Duncombe, J.: The surprising reach of Tonga's Giant atmospheric waves, Eos, 103, 2022.

Drob, D. P., Emmert, J. T., Meriwether, J. W., Makela, J. J., Doornbos, E., Conde, M., Hernandez, G., Noto, J., Zawdie, K. A., McDonald, S. E., Huba, J. D., and Klenzing, J. H.: An update to the Horizontal Wind Model (HWM): The quiet time thermosphere, Earth and Space Science, 2, 301–319, 2015.

Fritts, D. C., and Alexander, M. J.: Gravity wave dynamics and effects in the middle atmosphere, Rev. Geophys., 41,1003, 2003.

Francis, S. H.: Acoustic-gravity modes and large-scale traveling ionospheric disturbances of a realistic, dissipative atmosphere, J. Geophys. Res., 78 (13), 2278– 2301,1973.

Ghent, J. N., and Crowell, B. W.: Spectral characteristics of ionospheric disturbances over the southwestern Pacific from the 15 January 2022 Tonga eruption and tsunami, Geophysical Research Letters, 49, 2022.

Gusman, A.R., Roger, J., Noble, C. et al. The 2022 Hunga Tonga-Hunga Ha'apai Volcano Air-Wave Generated Tsunami, Pure and Applied Geophysics, 2022.

Hersbach, H., Bell, B., Berrisford, P., Hirahara, S., Horányi, A.,Muñoz-Sabater, J., Nicolas, J., Peubey, C., Radu, R., Schepers, D., Simmons, A., Soci, C., Abdalla, S., Abellan, X., Balsamo, G., Bechtold, P., Biavati, G., Bidlot, J., Bonavita, M.,De Chiara, G., Dahlgren, P., Dee, D., Diamantakis, M., Dragani, R., Flemming, J., Forbes, R., Fuentes, M., Geer, A., Haimberger, L., Healy, S., Hogan, R. J., Hólm, E., Janisková, M.,Keeley, S.,

https://doi.org/10.5194/egusphere-2023-2429
Preprint. Discussion started: 27 October 2023

Laloyaux, P., Lopez, P., Lupu, C., Radnoti, G., deRosnay, P., Rozum, I., Vamborg, F., Villaume, S., and Thépaut, J. N. The ERA5 global reanalysis, Q. J. R. Meteorol. Soc., 146, 1999–2049, 2020.

Hickey, M. P., Schubert, G., and Walterscheid, R. L.: Propagation of tsunami-driven gravity waves into the thermosphere and ionosphere, J. Geophys. Res., 114, 2009.

Hickey, M. P., Schubert, G., and Walterscheid, R. L.: Atmospheric airglow fluctuations due to a tsunami-driven gravity wave disturbance, Journal of Geophysical Research, 115(A6), A06308, 2010.

Hines, C.: Gravity waves in the atmosphere, Nature, 239 (5367), 73–78, 1972.

Inchin, P. A., Heale, C. J., Snively, J. B., and Zettergren, M. D.: The dynamics of nonlinear atmospheric acoustic-gravity waves generated by tsunamis over realistic bathymetry, Journal of Geophysical Research: Space Physics,125, 2020.

Inchin, P. A., Heale, C. J., Snively, J. B., and Zettergren, M.D.: Numerical modeling of tsunami-generated acoustic-gravity waves in mesopause airglow, Journal of Geophysical Research: Space Physics,127, 2022.

Kanamori, H., and Given, J. W.: Lamb pulse observed in nature, Geophys. Res. Lett, 10, 373–376, 1983.

Koketsu K. and Higashi S.: Three-dimensional topography of the sediment/basement interface in the Tokyo Metropolitan area, Central Japan, Bull. seism. Soc. Am., 82, 2328-2349, 1992.

Kubota, T., Saito, T., & Nishida, K.: Global fast-traveling tsunamis driven by atmospheric Lamb waves on the 2022 Tonga eruption, Science, 377, 91-94, 2022.

https://doi.org/10.5194/egusphere-2023-2429
Preprint. Discussion started: 27 October 2023

Li, X., Ding, F., Yue, X., Mao, T., Xiong, B., and Song, Q.: Multiwave structure of traveling ionospheric disturbances excited by the Tonga volcanic eruptions observed by a dense GNSS network in China, Space Weather, 21, 2023.

Lighthill, M. J.: Waves in Fluids, Cambridge University Press, Cambridge, UK, New York, 504 pp.. ISBN: 0-521-01045-4, 1978.

Lin, J.-T., Rajesh, P. K., Lin, C. C. H., Chou, M.-Y., Liu, J.-Y., Yue, J., et al. Rapid conjugate appearance of the giant ionospheric Lamb wave signatures in the northern hemisphere after Hunga-Tonga volcano eruptions, Geophysical Research Letters, 49, 2022.

Lindzen, R. S., and Blake, D.: Lamb waves in the presence of realistic distributions of temperature and dissipation, Journal of Geophysical Research, 77(12), 2166–2176, 1972.

Li, Q., Xu, J., Liu, H., Liu, X., and Yuan, W.: How do gravity waves triggered by a typhoon propagate from the troposphere to the upper atmosphere?. Atmos. Chem. Phys., 22, 12077–12091, 2022.

Liu, H.-L., Wang, W., Huba, J.D., Lauritzen, P. H., and Vitt, F. Atmospheric and Ionospheric Responses to Hunga-Tonga Volcano Eruption Simulated by WACCM-X, Geophysical Research Letters, 2023.

Liu, X., Xu, J., Yue, J., and Kogure, M.: Strong gravity waves associated with Tonga volcano eruption revealed by SABER observations, Geophysical Research Letters, 49, 2022.

Makela, J. J., Lognonné, P., Hébert, H., Gehrels, T., Rolland, L., Allgeyer, S., et al. Imaging and modeling the ionospheric airglow response over Hawaii to the tsunami generated by the Tohoku earthquake of 11 March 2011, Geophysical Research Letters, 38 (24), 2011.

https://doi.org/10.5194/egusphere-2023-2429
Preprint. Discussion started: 27 October 2023

Occhipinti, G., Rolland, L., Lognonné, P., and Watada, S.: From Sumatra 2004 to Tohoku-Oki 2011: The systematic GPS detection of the ionospheric signature induced by tsunamigenic earthquakes, Journal of Geophysical Research: Space Physics, 118, 3626–3636, 2013.

Peltier, W., and Hines, C.: On the possible detection of tsunamis by a monitoring of the ionosphere, Journal of Geophysical Research, 81(12), 1995–2000, 1976.

Pradipta, R., Carter, B. A., Currie, J. L., Choy, S., Wilkinson, P., Maher, P., and Marshall, R.: On the propagation of traveling ionospheric disturbances from the Hunga Tonga-Hunga Ha'apai volcano eruption and their possible connection with tsunami waves. Geophysical Research Letters, 50, 2023.

Salmon, R.: Introduction to ocean waves, Scripps Inst. of Oceanogr., Univ. of Calif., San Diego., 2014.

Smith, S.M., Martinis, C. R., Baumgardner, J., and Mendillo, M.: All-sky imaging of transglobal thermospheric gravity waves generated by the March 2011 Tohoku Earthquake, J. Geophys. Res. Space Physics,120, 10,992–10,999, 2015.

Symons, G. J.: The Eruption of Krakatoa, and Subsequent Phenomena: Report of the Krakatoa Committee of the Royal Society (Wiley Online Library), 1888.

Themens, D. R., Watson, C., Zagar, N., Vasylkevych, S., Elvidge, S., McCaffrey, A., et al. Global propagation of ionospheric disturbances associated with the 2022 Tonga volcanic eruption, Geophysical Research Letters, 49(7), 2022.

Vadas, S. L., Makela, J. J., Nicolls, M. J., and Milliff, R. F.: Excitation of gravity waves by ocean surface wave packets: Upward propagation and reconstruction of the thermospheric gravity wave field, J. Geophys. Res. Space Physics,120, 9748–9780, 2015.

Wright, C.J., et al. Surface-to-space atmospheric waves from Hunga Tonga-Hunga Ha'apai eruption, Nature, 609 (7928), 741–746, 2022.

Xu, J., Li, Q., Sun, L., Liu, X., Yuan, W., Wang, W., Yue, J., Zhang, S., Liu, W., Jiang, G., Wu, K., Gao, H., and Lai, C.: The Ground‐Based Airglow Imager Network in China: Recent Observational Results, Geophysical Monograph Series, 261, 365-394, 2021.

Xu, J., et al. Concentric gravity waves over northern China observed by an airglow imager network and satellites, J. Geophys. Res. Atmos.,120,11,058–11,078, 2015.

Yamada, M., Ho, T.-C., Mori, J., Nishikawa, Y., and Yamamoto, M.-Y.: Tsunami triggered by the Lamb wave from the 2022 Tonga volcanic eruption and transition in the offshore Japan region, Geophysical Research Letters, 49, 2022.

Yeh, K. C., and Liu, C. H.: Acoustic-Gravity Waves in the Upper Atmosphere, Reviews of Geophysics and Space Physics, 12 (2), 193, 1974.

Wrasse, C. M., Nakamura, T., Tsuda, T., Takahashi, H., Medeiros, A. F., Taylor, M. J., Gobbi, D., Salatun, A., Suratno, E. A., and Admiranto, A. G.: Reverse ray tracing of the mesospheric gravity waves observed at 23°S (Brazil) and 7°S (Indonesia) in airglow imagers, J. Atmos. Sol. Terr. Phys., 68, 163– 181, 2006.

Zhang, S., Vierinen, J., Aa, E., Goncharenko, L. P., Erickson, P., Rideout, W., et al. 2022 Tonga volcanic eruption induced global propagation of ionospheric disturbances via Lamb waves, Frontiers in Astronomy and Space Sciences, 9, 1–10, 2022.